URTeC: 2693686

Can Moment Tensor Inversion Aid Engineering Decisions? A Delaware Basin Case Study

Mark G. Mack[2], Scott M. Taylor[2], Jamie Rich[1], Dan Kahn[1], Jeremy King[2], Ben Schaeffer[2], Anton Reshetnikov[3], David Langton[1], Brendan Elliott[1], Alex Biholar[1]
[1] Devon, [2] Sigma Cubed, [3] Fracture Imaging

This paper was prepared for presentation at the Unconventional Resources Technology Conference held in Austin, Texas, USA, 24-26 July 2017.

Summary

A 22-stage horizontal well stimulation treatment in the Delaware Basin was monitored with three microseismic arrays. The results of advanced processing of the microseismic data were used to evaluate well spacing and completion designs and to estimate the local stress field.

The paper shows that well observed and appropriately processed microseismic data can provide valuable information for engineering decision and designs. Advanced processing such as Moment Tensor Inversion and Microseismic Reflection Imaging add significant value relative to conventional microseismic processing.

Preferential fracture propagation toward a previously produced well was observed in both the microseismic data and the offset well pressure data. Inefficient stimulation of such previously-depleted rock can be detected in real time using microseismic moment. Observations of inefficient stimulation can be used to modify job designs, both in the field in real time and in pre-job planning.

Natural fractures orientations were identified through Moment Tensor Inversion analysis, and it was noted that one completion design induces more microseismic activity than others, and tended to activate one fracture set more than the other.

Depletion-induced changes in the stress field orientation around the produced well were observed in both Moment Tensor Inversion and Microseismic Reflection Imaging. Importantly, these two techniques are independent.

It is also proposed that stimulation designs can be modified based on observations of drilling gas shows which impact fracture extent.

Introduction

A horizontal well in the Permian Basin was stimulated with a 22-stage hydraulic fracturing treatment. The job was monitored with two vertical microseismic arrays and one horizontal array in adjacent wells, shown in Figure 1. Although the entire job was monitored, this paper focuses on the advanced processing of the results for the last six stages, also indicated in the figure. One of the adjacent wells (the parent well) had previously been on production. Pressure was monitored in this well via a downhole gauge.

This paper addresses three specific objectives of the monitoring project, i.e.,

1. Well spacing, including the impact of a nearby depleted well.
2. Comparison of three different treatment designs (Denoted as Design Types A, B and C in this paper).
3. Stress estimation.

Figure 2 shows the overall microseismic event dataset colored by Stimulation Design Type. Qualitatively, growth appears to be asymmetric toward the previously-produced parent well, and Design Type B appears to show more extensive growth than Types A and C. Downward growth out of zone was minimal, and some upward growth is indicated, except for a few stages.

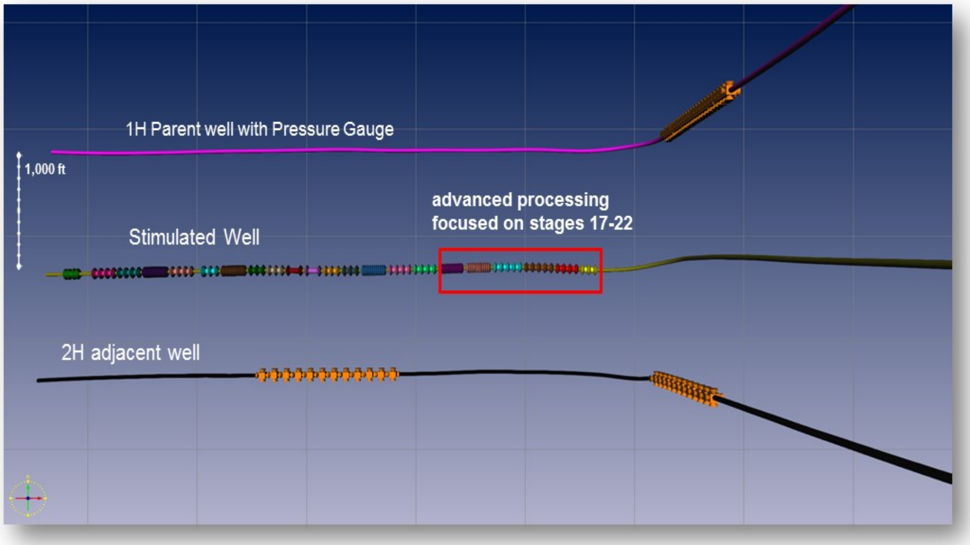

Figure 1. Overview of 22 stage treatment monitored with two vertical microseismic arrays and one horizontal array.

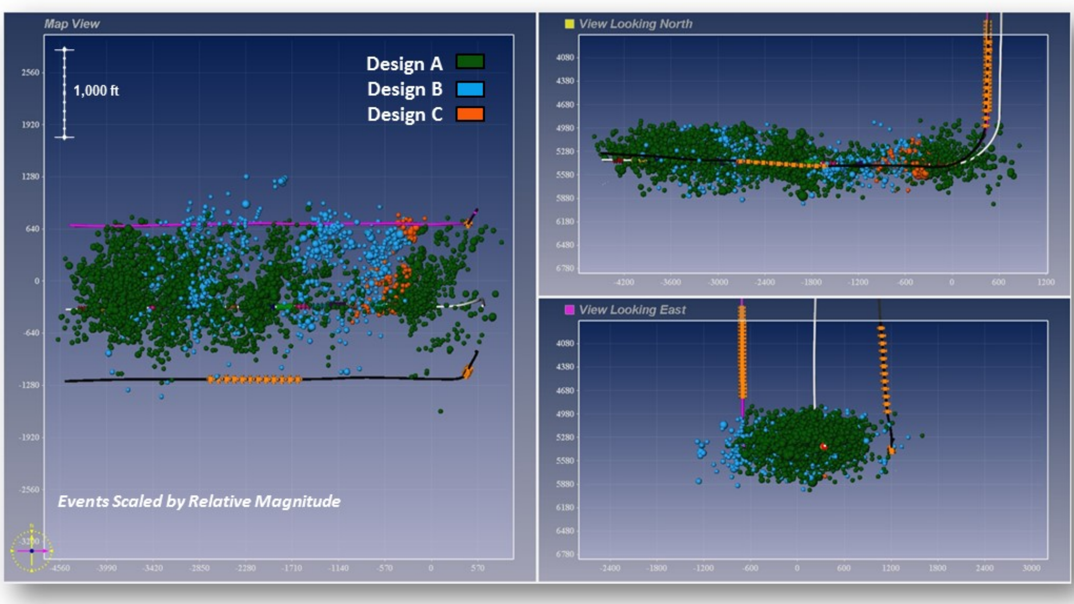

Figure 2. Overview of all microseismic data colored by Completion Design Type. Type B completions appear to generate larger event clouds.

Well Spacing Analysis

The wells in this area were 1000 ft apart, and one of the three wells in this study had been previously produced. The pressure in this parent well was monitored to determine whether the stimulation of the offset well interacted with the parent well. Figure 3 shows the pressure in the parent well, with the pumping start and stop times superimposed.

The plot of the overall job shows small pressure increases for most stages and a few larger increases. We hypothesize that the magnitude of the pressure increases indicates the quality of the connection between the fracture networks in the two wells, with the large spikes representing direct hits and the smaller ones representing less direct connections, possibly through natural fractures or poroelastic effects.

Figure 4 shows the same data, with each day broken out separately. The pressure scales have been expanded to better identify the start of the pressure increases. It can be noted that the pressure increase generally occurs after the start of pumping, with a typical lag of 25 minutes after full rate has been achieved. There was some correlation between the pump time and the magnitude of the pressure increase, as shown in Figure 5. In particular, the three largest pressure hits were all associated with longer pump times. The stages which produced the largest hits were pumped into sections of the lateral with relatively high drilling gas shows, so it is not possible from this analysis to determine whether the pressure hits were caused by the larger jobs or if there were more conductive pathways to the parent well, either due to the parent well stimulation or natural permeability streaks.

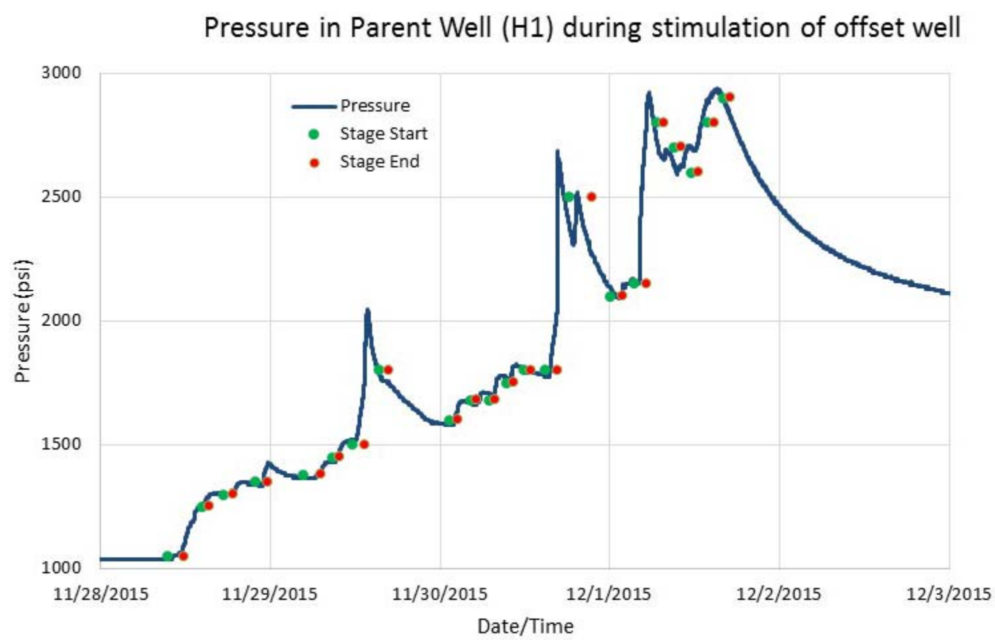

Figure 3. Pressure in parent well during stimulation of offset well shows generally rising pressure and time delay between start of pumping in offset well and pressure increment in parent well.

Figure 4. Expanded view of parent well pressure data shown in Figure 3.

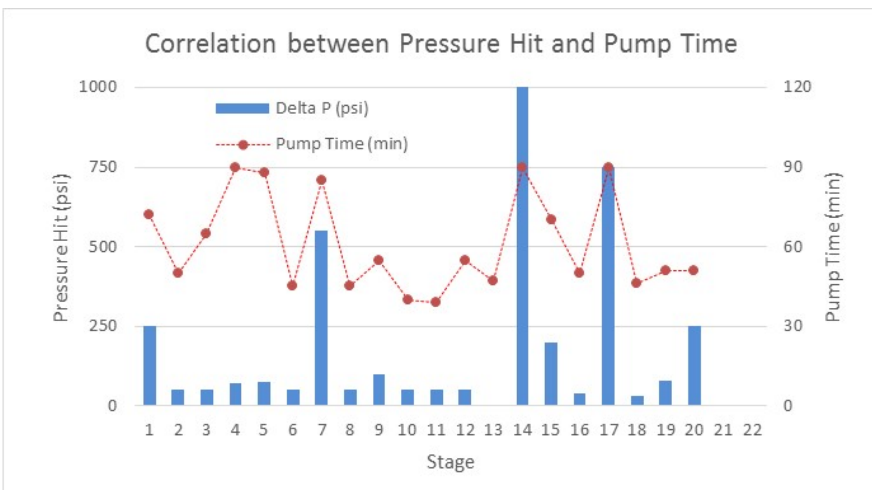

Figure 5. The pressure increase in the parent well was somewhat correlated with the pump time into the offset well.

Microseismic data was also used to investigate the impact of neighboring depleted wells on fracture geometry and stimulation effectiveness. The moment of a microseismic event is related to the magnitude, and is a measure of the energy released during the event. The Cumulative Moment is the sum of the moment of all the events over a specified time and volume. Figure 6 shows the Cumulative Moment of the microseismic activity on each side of the well, together with the pumping data for the completion stages in this study.

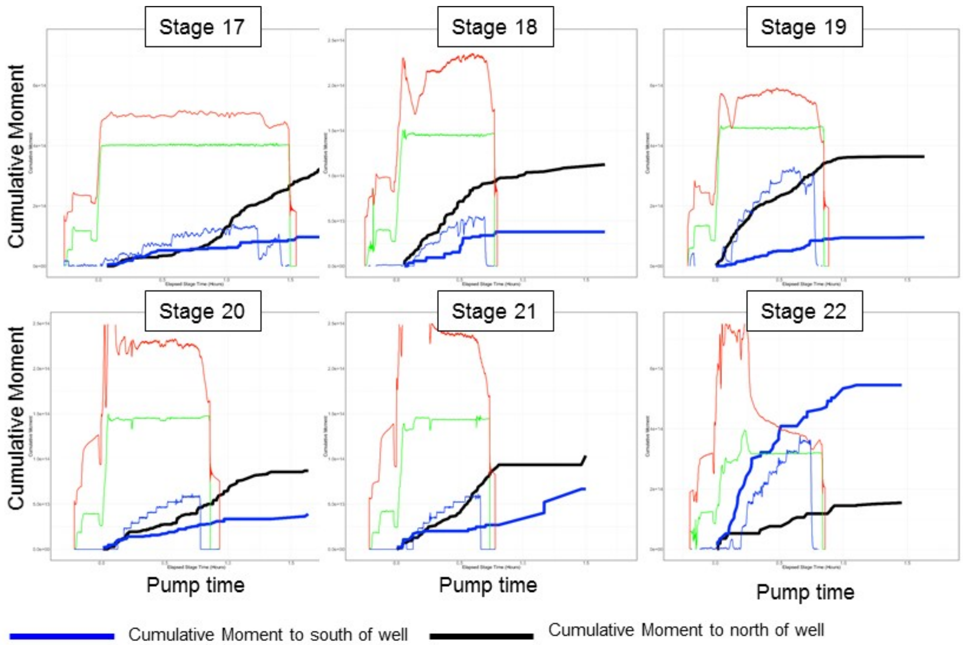

Figure 6. Cumulative Moment as a function of time showing more activity toward the depleted parent well for stages that interact with the parent well.

In Stage 17, the Cumulative Moment is very similar on each side of the well for the first 45 minutes of pumping. After 45 minutes, the activity moves toward the parent well on the north side, indicating that the fracture is growing predominantly in that direction. It has previously been shown (Mack et al, 2016) that depletion lowers the stress around a producing well, such that hydraulic fractures grow preferentially toward the depleted well. Stage 17 was a Design B stage, and also exhibited a large pressure hit in the parent well. Figure 7 shows the fracture propagation curve for Stage 17. This is similar to the so-called R-t plot (Shapiro and Dinske, 2009), modified to represent the fracture front rather than the diffusion front. This plot indicates that a planar fracture should reach the parent well after about 35 minutes. If this were the case, the cumulative moment would have begun to deviate earlier, because the depleted zone is reached before the fracture reaches the parent well. This suggests that the propagation rate is slower than predicted by the planar fracture front model, which may be an indication of fracture complexity.

In Stage 21, growth was initially toward the parent well, but the latest events in the stage (after pumping ended) were on the opposite side. There were insufficient late events to draw a definitive conclusion but one potential explanation of the late activity is that this stage near the heel was less affected by the depletion around the parent well than other stages were. (The fracture azimuth is approximately 35 degrees east of north.) It may have grown out of the depleted area, which would then encourage growth to revert to the opposite side.

Stage 22 showed the reverse of the majority of stages in the job, with more activity to the south than the north. The location of this stage was outside the depleted area to the north. Geomechanical models show that there is a higher stress zone adjacent to the lower-stress depleted zone. In addition, it is possible that the previous stages which grew to the north created a stress shadow which would suppress fracture growth in that direction.

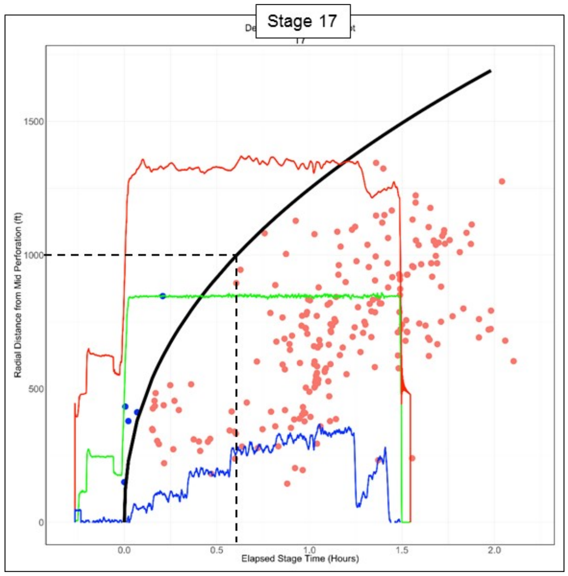

Figure 7. Fracture front predicted to reach parent well after 35 minutes.

A third technique to assess well spacing in the presence of depletion is Microseismic Reflection Imaging (MRI, Reshetnikov, 2013), described in detail in Appendix A. In essence, this technique uses the detailed waveforms of events in a stage to detect surfaces created by previous stages, similar to the detection algorithms in surface seismic. During stimulation, these surfaces can be interpreted as areas of changed material properties, indicating the presence of disturbed volumes which may be hydraulic fractures.

Figure 8 shows the MRI results for Stage 17. In extremely low permeability formations, the depleted zone does not extend far from the stimulated volume. The clear change in the orientation of the interpreted volumes approximately 500 ft from the stimulated well most likely indicates the extent of the depletion.

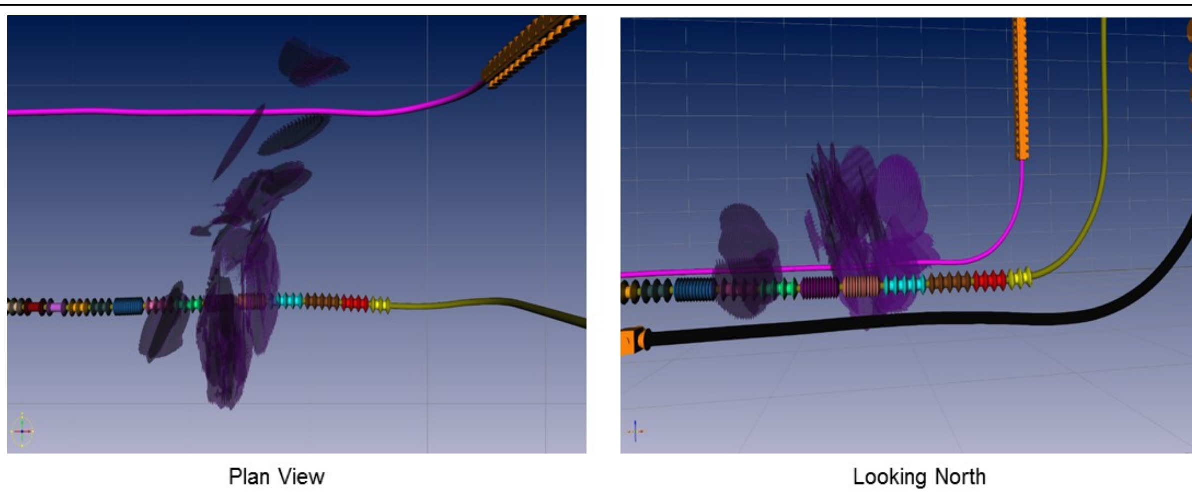

Figure 8. Microseismic Reflection Imaging shows a distinct reorientation near the edge of the depleted zone.

Completion Design Analysis

One of the primary objectives of this work was to assess the benefit of completion design changes. The majority of the well was stimulated with a Design A Completion. Stage 17 was one of the stages designated as a Design B, and Stage 18 was a Design C. Stages 19 – 22 were all the standard Design A.

It has already been noted that microseismic activity during the Design B completion extended further laterally than the other types. Design B also generally created larger pressure hits than the other designs. Design B used a higher volume of a thinner fluid, which may explain the pressure hits and microseismic extent.

Moment Tensor Inversion (MTI) analysis was performed for the six stages in this study. MTI analysis yields the orientation of the slip plane and the direction of slip. Individual events are represented by the symbol in Figure 9, i.e., a ball inside a disk with an arrow on the disk. The ball indicates the event location (sometimes sized proportionally to event magnitude), the disk represents the orientation of the slip plane, and the arrow represents the direction of slip, as shown in Figure 9. Appendix B describes the methodology in more detail.

Figure 10 shows the MTI results for one set of events during one stage. This presentation can highlight spatial differences but it can be challenging to interpret a large number of events. It may be easier to understand rose diagrams or stereonets instead. Figure 11 shows the rose diagrams of event azimuth for the six stages, and Table 1 summarizes the results. There are several important observations, i.e.,

1. The events did not align with the aggregate microseismic event cloud orientation. This implies that the slip planes were not aligned with the preferred direction of fracture propagation.
2. In stages 18 – 20, there were two distinct sets of events, with different orientations. These stages also exhibited higher treating pressures than the other stages.
3. Stage 17 (Design Type B) tended to activate one set preferentially. It also triggered more microseismic activity than the other stages.
4. Stage 22 appeared to preferentially activate the other set. This is the stage which grew preferentially to the south rather than the north, and was not impacted by depletion.

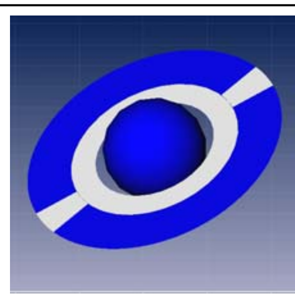

Figure 9. Moment tensors are represented by a ball inside a disk with an arrow on the disk. The ball indicates the event location (sometimes sized proportionally to event magnitude), the disk represents the orientation of the slip plane, and the arrow represents the direction of slip.

Stage	**Completion Type**	**Treating Pressure (psi)**	**Set 1 Event Orientation (deg from north)**	**Set 2 Event Orientation (deg from north)**
17	B	5500	+20	-27
18	C	6300	+20	-29
10	A	6300	+22	-27
20	A	6300	+22	-39
21	A	5000	+23	-33
22	A	5500	+20	-20

Table 1. Summary of event orientations and treating pressures.

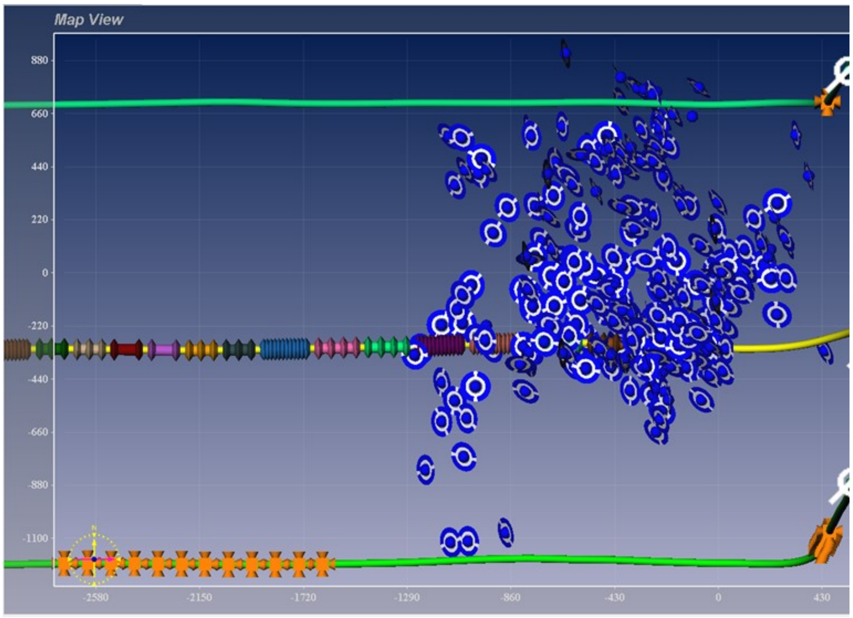

Figure 10. Moment Tensor results for one set of events in one stage.

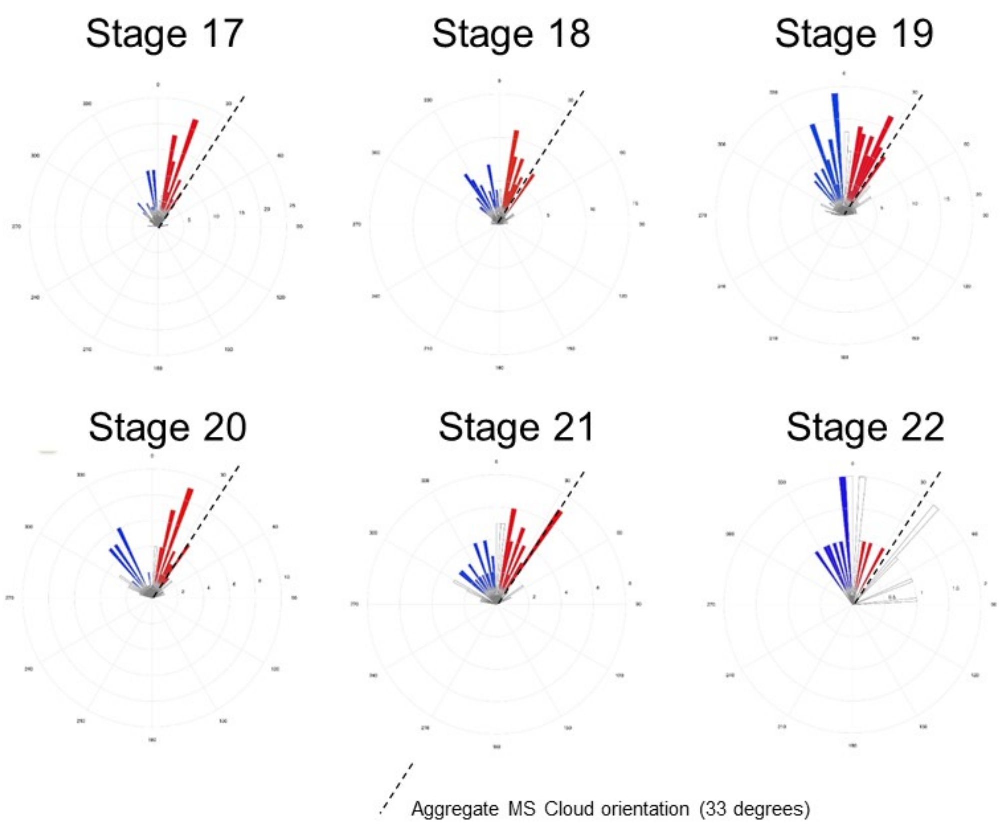

Figure 11. Rose diagram of azimuth of events for the six stages in this case study.

Mohr's Circle Analysis of Completion Design

The MTI results can be used to gain a more quantitative understanding of the completion designs. Prior to fracturing, both the rock matrix and the natural fractures are in a stable mechanical state, such as that shown in Figure 12a. Near the fracture tip, the rock and fractures can be destabilized by the stress changes caused by the propagating fracture, as shown in Figure 12b. However, close to the fracture but behind the tip, the minimum stress is increased by an amount equal to the net pressure in the fracture at that point. This stabilizes the rock and natural fractures, as shown in Figure 12c. Figure 13 (from Maxwell et al, 2015) shows the region around the tip in which natural fractures can fail. The authors showed that the size of that region depends on the orientation of the natural fracture set, the stress state and the mechanical properties of the natural fractures.

Failure can also occur if the fluid pressure increases in the natural fractures. The Coulomb failure criterion is based on the effective stress (stress minus pore pressure). Pressurizing natural fractures (with no other stress changes) is represented by shifting the Mohr's Circle to the left, as shown in Figure 12d.

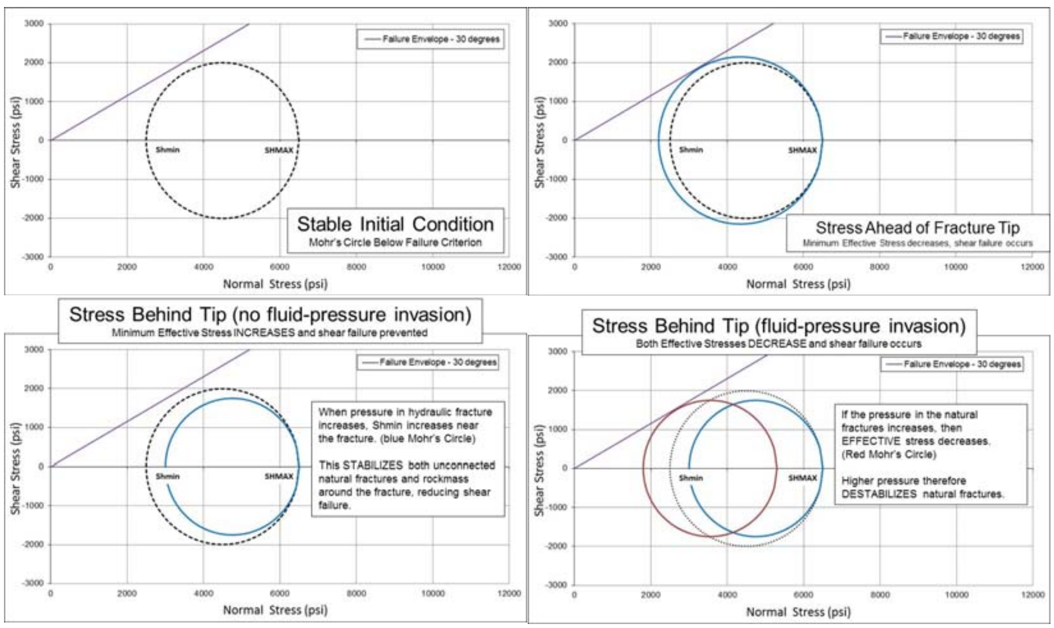

Figure 12. Mohr's Circle analysis showing stress (a) in stable initial condition, (b) ahead of fracture tip, (c) behind the fracture tip, and (d) accounting for fluid pressure invasion into natural fractures which can result in shear failure.

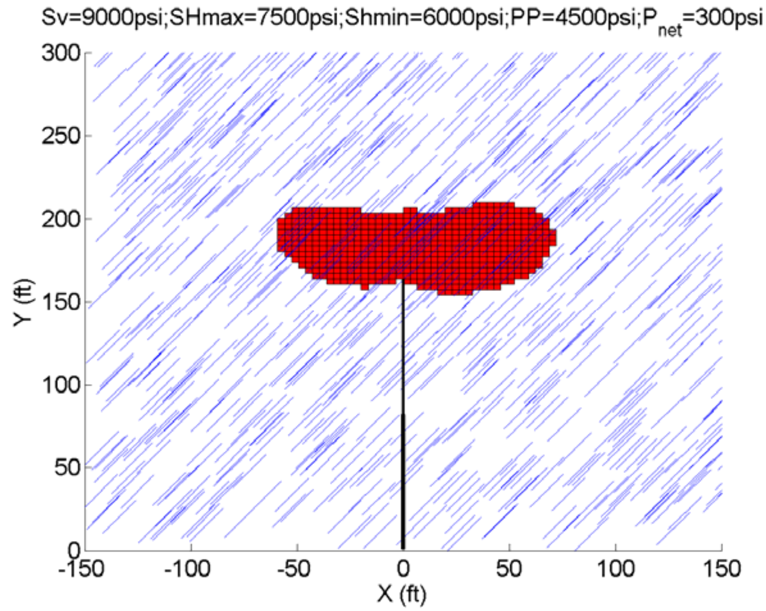

Figure 13. Fractures oriented in the direction of the blue lines fail in the region outlined in red.

The orientation of the local stress field can be inferred from the overall orientation of the microseismic cloud, and the orientation of the failure planes are a direct output of the MTI analysis. For an assumed local stress state, the normal and shear stresses on any plane are determined by the relative orientation of that plane to the principal stress directions. The plane orientations for the 6 stages in this paper are shown on the Mohr's Circle in Figure 14a, for one stress state and an assumed pore pressure of 3000 psi. In this case, only relatively weak fractures (friction angle of 20 degrees) can fail. On the other hand, Figure 14b shows that at a higher pressure, even stronger fractures (friction angle of 30 degrees) can fail in Set 1, and weaker fractures will fail in both Sets 1 and 2.

We hypothesize that the higher level of activity in Stage 17 (Design B) occurred because the thinner fluid in this stage could penetrate more easily and further into the fracture network, thus activating more fractures. Although the treating pressure was lower, the pressure in the natural fractures was higher, as in Figure 14b. On the other hand, the higher treating pressures associated with thicker fluids did not penetrate as deeply into the formation, resulting in a lower overall level of microseismic activity, but with the activity being both more equally divided between the two sets.

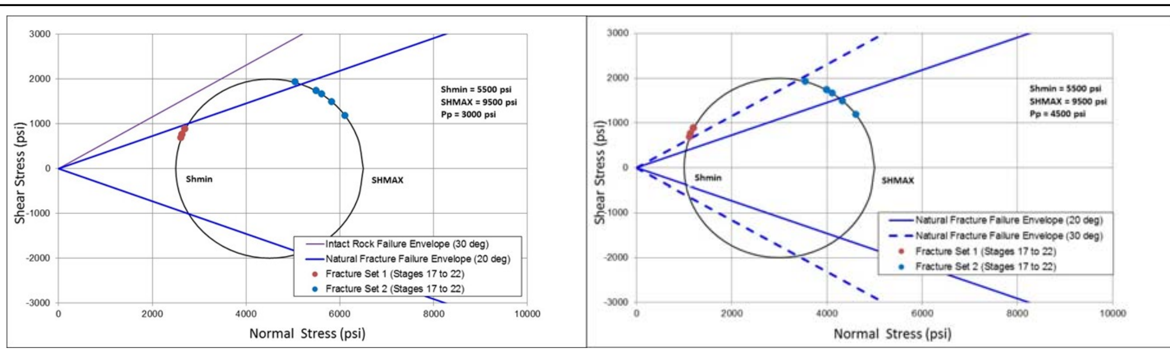

Figure 14. The plane orientations from Moment Tensor Inversion analysis indicate that at low natural fracture pressure (a), only weaker fracture fail in both sets of fractures. At higher natural fracture pressures (b) even stronger fractures fail, but one set fails preferentially

Stress State from Moment Tensor Analysis

Lacazette and Morris (2015) have developed a method to estimate stress from passive seismic data using slip tendency analysis. Their method was applied to the Moment Tensor Inversion data in this project, and the results are shown in Figures 15 through 17. Figure 15 shows the slip tendency plot derived from a subset of the data in this project, with the estimated stress directions and microseismic event orientations superimposed. Figure 16 shows the stresses at the events on a three-dimensional Mohr's Circle, and Figure 17 shows the events color-coded by slip tendency.

This analysis indicates that the major principal stress is vertical. The minor stress is not completely consistent with the orientation of the clouds used in the two-dimensional Mohr's Circle analysis in the previous section. We have not yet determined whether this is due to uncertainty in the method or if there is a geomechanical explanation of this effect, such as *en echelon* fractures combining to create a cloud which is not aligned with the principal stress direction.

The slip tendency plot provides the orientations and relative values of the principal stresses. Estimated values of the actual stresses can be obtained if one stress can be estimated independently. Frequently (including in this case), the maximum principal stress is vertical. The vertical stress is easily derived (e.g., from a density log) and can be used to extract the values of the other two principal stresses (the minimum and maximum horizontal stresses). One of the significant benefits of this technique is the ability to estimate the maximum horizontal stress, which is usually difficult to obtain by other methods.

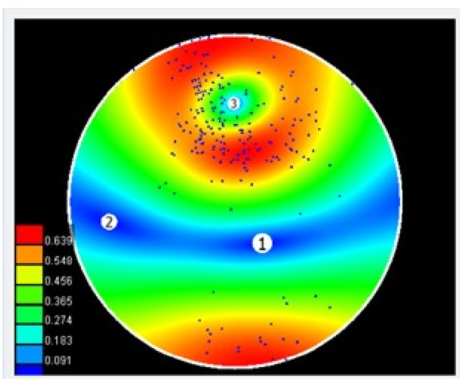

Figure 15. Slip tendency plot of one subset of the microseismic events.

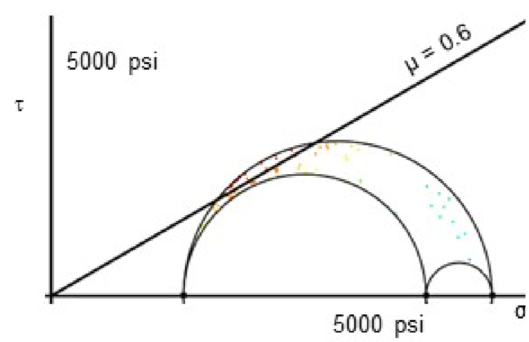

Figure 16. Microseismic events plotted on three-dimensional Mohr's Circle.

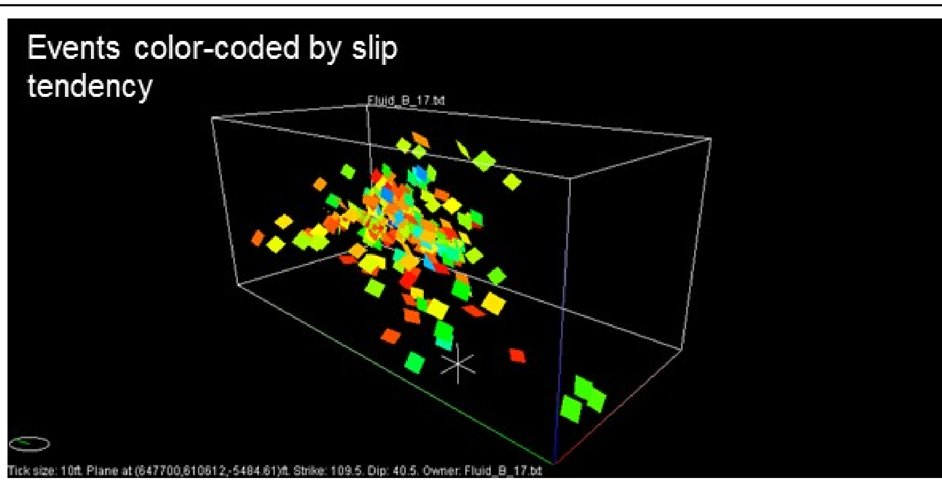

Figure 17. Microseismic events color-coded by slip tendency.

Conclusions

Offset well pressure data and frac hits can be used to calibrate hydraulic fracture models and the hydraulic fracture propagation front used in microseismic analysis. In this case study, the preferential propagation toward the previously produced well was validated by the microseismic data and frac hit pressure analysis.

Inefficient stimulation of previously-depleted rock can be detected in real time using microseismic moment. Job size can be reduced in the field when asymmetry is detected in the Cumulative Microseismic Moment. In addition, future jobs can be designed to account for the effect of a depleted parent well.

Natural fractures orientations were identified through Moment Tensor Inversion analysis. One completion design induces more microseismic activity than others, and also tended to activate one fracture set more than the other.

Depletion-induced changes in the stress field orientation around the produced well were observed in both Moment Tensor Inversion and Microseismic Reflection Imaging. This stress reorientation may cause offset well fractures to enhance production from the parent well, because repressurization during stimulation results in shear slip on previously unsheared planes.

Drilling gas shows and high permeability streaks were observed to impact fracture extent. Stimulation designs can be modified for sections of the lateral with these features.

Well observed and appropriately processed microseismic data can provide valuable information for engineering decision and designs. Advanced processing such as Moment Tensor Inversion and Microseismic Reflection Imaging add significant value relative to conventional microseismic processing.

References

Chapman, C. Fundamentals of seismic wave propagation. Cambridge University Press, 2004.

Lacazette, A. and Morris, A. A New Method of Neostress Determination From Passive Seismic Data. Unconventional Resources Technology Conference, San Antonio, Texas, 20-22 July 2015.

Mack, M., Zhang, F., Lee, B, Maxwell, S., Dohmen, T. and Cipolla, C. Geomechanical modeling of microseismic depletion delineation. SEG Technical Program Expanded Abstracts 2016.

Maxwell, S., Mack, M., Zhang, F., Chorney, D., Goodfellow, S. and Grob, M. Differentiating Wet and Dry Microseismic Events Induced During Hydraulic Fracturing. Unconventional Resources Technology Conference, San Antonio, Texas, 20-22 July 2015.

Oelke, A., Alexandrov, D. Abakumov, I., Glubokovskikh, S., Shigapov, R., Krüger, O., Kashtan, B., Troyan, V., and Shapiro, S. (2013) Seismic reflectivity of hydraulic fractures approximated by thin fluid layers. Geophysics, Vol. 78, NO. 4 P. T79–T87.

Reshetnikov, Anton. Microseismic reflection imaging. Diss. Freie Universitaet Berlin, 2013.

Shapiro, S. A., and Dinske, C.. "Fluid□induced seismicity: Pressure diffusion and hydraulic fracturing." Geophysical Prospecting 57.2 (2009): 301-310.

Vavryčuk, V. Moment tensor decompositions revisited. Journal of Seismology 19.1 (2015): 231-252.

Appendix A. Summary of Microseismic Reflection Imaging

The focus of Microseismic Reflection Imaging technology is to directly image both induced and naturally occurring sub-seismic natural fracture. This process migrates and images the reflected waves generated from microseismic data considering microseismic events as virtually controlled active seismic sources. Reflection-seismic imaging is a well-established approach widely applied in exploration seismology since the 1930s. Oelke et al (2013) described an application to hydraulic fracture imaging.

There are many migration algorithms based on different physical approximations and applicable to different types of seismic data. Nevertheless, microseismic data have a set of unique features that distinguish it from any other active seismic data. These features have to be taken into account in order to get a reasonable result for the given problem. Particularly, in contrast to active seismic, microseismic events are not controlled sources, though their location in the case of proper acquisition can be determined. Further, a quantitative bound on the error space or confidence can now be derived. Moreover, the area of interest is likely to be the same seismically active zone where microseismicity occurs. This means that microseismic sources are located in the direct vicinity of a target and at a distance from seismic sensors in contrast to surface, VSP and marine data where sources are at a distance from a target. Acquisition geometries used for microseismic monitoring are different from geometries of land seismic or VSP. Since the main purpose of microseismic monitoring is to detect the arrival times of events, the number of receivers in microseismic acquisition systems is usually much smaller and they are sparsely distributed. Among other limitations, this restricts applicability of any post-stack imaging. In some cases, amount of events can reach hundreds or even thousands, which is usually one or two orders of magnitude larger than the number of sensors.

The sources used in active seismic are different kinds of explosions, vibrators or air guns with well-known and in most cases spherical radiation patterns. On the other hand microseismic events are small earthquakes with complicated focal mechanisms, which might be initially unknown. These focal mechanisms as well as source energies can vary significantly even for events located close to each other. Furthermore, microseismic sources have higher frequency and lower energy signals compared to conventional seismic sources.

Appendix B Moment Tensor Inversion

Current Moment Tensor Inversion (MTI) methods take into account effects of anisotropy between source and receivers but ignore the effect of local anisotropy in the source and its influence on event radiation pattern.

The moment tensor inversion method used in this work takes into account effects of anisotropy in the source location (local anisotropy, Chapman, 2004) in addition to the inversion process through a fully 3D anisotropic model. Even moderate degrees of anisotropy can have a significant effect on the radiation pattern. Most other methods do not fully address this important issue, which can lead to significant inversion errors and an unreliable interpretation.

Furthermore, instead of inverting event moment tensor directly we invert for fault plane normal and slip direction vectors. This constrains the parameter range better and improves the reliability of the interpretation.

<u>Comparison with conventional MTI solutions</u>

A pure slip event embedded in an anisotropic medium can appear as an event with a strong non-DC component. Methods which ignore the effect of local anisotropy in the source and its influence on event radiation pattern thus lead to significant errors. In particular, an unrealistically large number of events with strong non-DC component are indicated and a chaotic distribution of radiation patterns is observed within a microseismic cloud.

In contrast, accounting for anisotropy in the source and between the source to receivers allows us to correctly compute synthetic amplitudes of all three wave types for any given source type and to get precise MTI solutions for anisotropic environments. The moment tensor is decomposed into DC and non-DC components (Vavrycuk, 2015) to facilitate the inversion process and to improve the classification and interpretation of microseismic sources. The inversion algorithm also resolves the ambiguity in identifying the fault plane on which actual slip occurred.